analytical chemistry

Article

pubs.acs.org/ac

Direct Measurements of Mass-Specific Optical Cross Sections of Single-Component Aerosol Mixtures

James G. Radney,[†,‡] Xiaofei Ma,[†,‡] Keith A. Gillis,[†] Michael R. Zachariah,[†,‡] Joseph T. Hodges,[†] and Christopher D. Zangmeister*[,†]

[†]Material Measurement Laboratory, National Institute of Standards and Technology, Gaithersburg, Maryland 20899, United States

[‡]Department of Mechanical Engineering and Department of Chemistry and Biochemistry, University of Maryland, College Park, Maryland 20742, United States

Supporting Information

ABSTRACT: The optical properties of atmospheric aerosols vary widely, being dependent upon particle composition, morphology, and mixing state. This diversity and complexity of aerosols motivates measurement techniques that can discriminate and quantify a variety of single- and multicomponent aerosols that are both internally and externally mixed. Here, we present a new combination of techniques to directly measure the mass-specific extinction and absorption cross sections of laboratory-generated aerosols that are relevant to atmospheric studies. Our approach employs a tandem differential mobility analyzer, an aerosol particle mass analyzer, cavity ring-down and photoacoustic spectrometers, and a condensation particle counter. This suite of instruments enables measurement of aerosol particle size, mass, extinction and absorption coefficients, and aerosol number density, respectively. Taken together, these observables yield the mass-specific extinction and absorption cross sections without the need to model particle morphology or account for sample collection artifacts. Here we demonstrate the technique in a set of case studies which involve complete separation of aerosol by charge, separation of an external mixture by mass, and discrimination between particle types by effective density and single-scattering albedo.

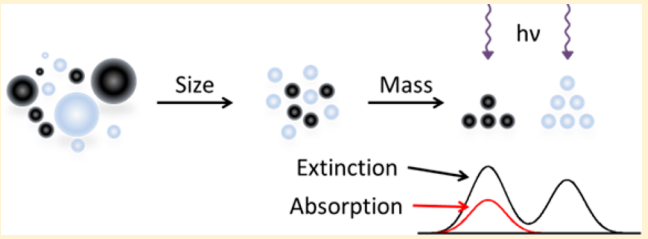

This study describes a new method for size- and mass-based separation of aerosol particles combined with optical characterization to yield mass-specific absorption and extinction cross sections. We foresee wide-ranging applications to nanomaterial systems where physical properties of component particles need to be quantified, such as in pharmaceutical manufacturing,[1] biomedical applications,[2] and the role of aerosols in atmospheric processes.[3] Here, our goal is to develop methods for measuring the optical properties of atmospheric aerosols that play a key role in the Earth's radiation budget. At present, a relatively large uncertainty in the radiative forcing of these aerosols motivates new strategies for laboratory and field measurements. A particularly important example is black carbon (BC), which comprises carbonaceous aerosols formed from combustion processes. Next to CO_2, BC is potentially the greatest anthropogenic contributor to global warming.[4] However unlike CO_2, BC has a brief residence time in the atmosphere, and consequently the mitigation of BC emissions could be used to slow climate change on a short time scale.[5]

Quantifying the effect of BC on the radiation budget of the Earth requires accurate knowledge of the physical and chemical properties and the concomitant ability to model the radiative effects of BC. The mass absorption cross section (MAC), mass scattering cross section (MSC), and single-scattering albedo (ω_0) are inputs to global climate models, where

$$\omega_0 = \frac{\mathrm{MSC}}{\mathrm{MAC} + \mathrm{MSC}} \tag{1}$$

Incorrect parametrization of these values may lead to unacceptable errors in the calculation of radiative forcing.[4b]

The MAC and MSC represent the mass-specific absorption and scattering cross sections, respectively. For the MAC we find

$$\mathrm{MAC} = \frac{\alpha_{\mathrm{abs}}}{M} = \frac{\alpha_{\mathrm{abs}}}{V\rho N} = \frac{\alpha_{\mathrm{abs}}}{m_{\mathrm{p}}N} = \frac{C_{\mathrm{abs}}}{m_{\mathrm{p}}} \tag{2}$$

where M is the mass concentration of the aerosol particles in air, and α_{abs} is the absorption coefficient, which represents the fractional loss by absorption in light intensity per unit propagation distance. The term α_{abs} is equal to NC_{abs}, where C_{abs} is the particle absorption cross section and N is the particle number density. Depending upon the observables, MAC can also be defined in terms of N, with the particle volume V and the particle mass density ρ, or with the average particle mass m_{p}. Identical equations for scattering and extinction can be defined by replacing α_{abs} with α_{scat} and α_{ext}, respectively, where we note that extinction is the sum of absorption and scattering.

Received: June 3, 2013
Accepted: July 22, 2013
Published: July 22, 2013

   dx.doi.org/10.1021/ac401645y | Anal. Chem. 2013, 85, 8319−8325

Filter-based measurements determine the MAC or MEC (mass extinction cross section) of aerosols through the first definition of eq 2. With this approach a known volume of air, given by V_a, is sampled through a filter, and the total mass of particles deposited onto the filter, m_{tot}, is measured to yield $M = m_{tot}/V_a$. The absorption or extinction coefficient is subsequently obtained by measuring the change in filter transmission using an aethalometer or a particle soot absorption photometer.[6] These types of filter measurements are relatively common because they are robust, inexpensive, and simple to perform. The ubiquity of the resulting data facilitates statistical analyses and measurement intercomparisons. Filter-based techniques can also incorporate particle size selection using cascade impactors that separate particles into flow-rate-dependent size bins. However, we note that the typical size resolution is relatively coarse, with only a few bins spanning the entire spectrum. Also, filter measurements require long exposure times (hours to days) to collect enough sample for gravimetric analysis. Large differences in mass concentration have been observed when the BC mass fraction is low[4b,7] consistent with large uncertainties caused by evaporative mass loss or adsorptive mass gain.[8]

Aerosol MACs have also been determined by measuring the optical properties and inferring the mass concentration[9] or particle density.[10] Optically, these measurements are rather robust, but the determination of mass concentration (typically from a filter measurement) or density (from the literature) is prone to error. In some instances, the mass concentration is determined in real time using a single particle soot photometer (SP2),[11] which is an instrument that measures the mass concentration of BC through laser-induced incandescence. Particles that do not incandesce, i.e. weakly absorbing and nonabsorbing particles, are not included in the mass concentration measurement. Failure to account for this selectivity toward BC can increase the uncertainty in the measurement of MAC in these multicomponent mixtures.[12]

The results presented below represent a direct measurement of MAC and MEC through particle separation by mass and density and independent determinations of optical cross sections. We use an experimental setup that comprises five distinct measurement stages: a differential mobility analyzer (DMA), an aerosol particle mass analyzer (APM), a cavity ring-down (CRD) spectrometer, a photoacoustic (PA) spectrometer, and a condensation particle counter (CPC). Importantly, the CRD, PA, APM, and CPC instruments provide direct measurements of α_{ext}, α_{abs}, m_p, and N, respectively. These measured values can be combined in eq 2 to yield aerosol MAC and MEC. This technique overcomes the aforementioned limitations of filter-based methods and requires no prior assumptions about mass concentration. Direct, in situ measurements are crucial for BC which has a low effective density by virtue of its fractal morphology.

In the remainder of this article we present laboratory measurements of the MAC, MEC, and the effective density of several atmospherically relevant aerosols. First, we demonstrate how the combination of particle mobility and mass separation techniques enables discrimination between particles of the same electrical mobility but different charge. Second, we show that this approach can be used to separate externally mixed aerosols by mass and that the addition of optical measurements enables discrimination and measurement of mass-specific, component optical cross sections.

MATERIALS AND METHODS

DMA-APM Measurement Technique. The DMA size-selects particles based upon their electrical mobility, Z, within an electric field according to[13]

$$Z = \frac{qeC(D_m)\chi}{3\pi\mu D_m} \tag{3}$$

where D_m is the particle mobility diameter, q is the number of elementary charges on the particle, e is the elementary charge ($e \approx 1.602 \times 10^{-19}$ C), μ is the viscosity of air, and $C(D_m)$ is the Cunningham slip-correction factor. The term χ, which is unity for spheres, is the dynamic shape factor and accounts for shape-dependent aerodynamic drag. It represents the ratio of the drag force on the particle to the drag on a spherical particle having the same volume.[14] In the case of salt aerosols, χ depends upon particle generation and aging conditions with values ranging from 1.02 to 1.26.[15] For soot particles, the value of χ increases from 1.1 to 2.2 as D_m increases from 50 to 220 nm.[16]

Since the DMA separates particles based upon electrical mobility, there is a class of larger particles with higher-order charges and the same apparent mobility diameter that will not be separated. Incorporation of a neutralizer to redistribute particle charge and a second DMA downstream of the first DMA can be used to separate overlapping size classes. However, the charge distribution imparted by the neutralizer is a function of particle diameter and must be estimated from the statistics of charge equilibrium. Further, even under these conditions a small fraction of the larger particles will maintain their original electrical mobility.

Herein, we use an APM to separate by mass an aerosol stream that has been size selected with a DMA, thus obviating the need for a second neutralizer and DMA. Briefly, the APM consists of two cylindrical electrodes forming an annular region in which the aerosol stream is introduced. The inner electrode is maintained at a voltage, V, with respect to a grounded outer electrode. Both electrodes rotate together at an angular velocity ω. Particles of a given mass are selected by the APM when they have a stable trajectory defined by the balance between centrifugal and electrostatic forces. These particles satisfy[17]

$$m_p r\omega^2 = \frac{qeV}{r \ln(r_2/r_1)} \tag{4}$$

where r, r_1, and r_2 correspond to the radii locating the center of the mass-classification space, the inner electrode, and outer electrode, respectively. With the rotation speed of the electrodes held constant, the selected particle mass is a function of the applied voltage. Notably, the center of the mass-classification space, r, is independent of particle shape.

Combining eqs 3 and 4 and assuming constant qe, then

$$m_p \propto \frac{ZD_m}{C(D_m)\chi} \tag{5}$$

Consequently, particles that have the same electrical mobility, Z, but different mobility diameters, D_m, (i.e. the q = 1, 2, 3... cases) will be separated by placing an APM after a DMA. In the limiting case where the drag coefficient, $C(D_m)\chi$, is large, as is possible with irregularly shaped particles, complete separation in mass space may not be possible. However, the addition of an optical measurement downstream of the mass separation often provides additional information to discriminate these over-

dx.doi.org/10.1021/ac401645y | Anal. Chem. 2013, 85, 8319−8325

lapping sizes. Further details of this size and mass separation procedure can be found in the Supporting Information.

This configuration also enables separating particles that have the same mobility diameter and selecting by effective density defined as

$$\rho_{\text{eff}} = \frac{6m_{\text{p}}}{\pi D_{\text{m}}^3} \tag{6}$$

Similar measurements for the determination of effective density have been performed.[18]

Aerosol Generation and DMA-APM-CRD-CPC Setup. The technique presented herein involves a DMA-APM-CRD/PA-CPC instrumental setup as shown in Figure 1. To produce

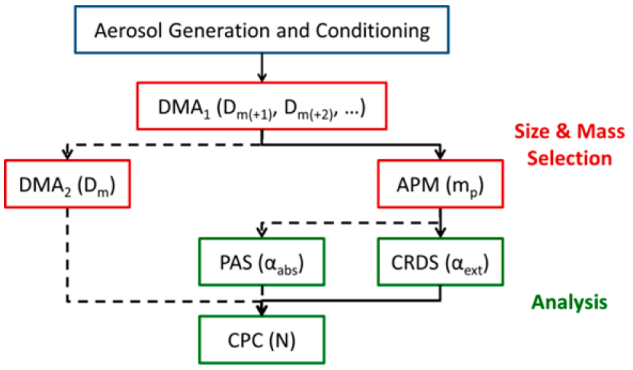

Figure 1. Block diagram of size and mass selection and particle analysis components. The measurements associated with each system component are shown in parentheses. Dashed lines indicate optional paths.

single aerosols for measurement, a liquid jet cross-flow (LJCF) atomizer (TSI 3076 constant output atomizer, 30 psi)[19] was used and aerosols were conditioned using two diffusion dryers (TSI 3062)[19] and a tube furnace (Lindberg/Blue Mini-Mite).[19] For production of externally mixed aerosols, two LJCF atomizers were used; the second atomizer was home-built. These two-component mixtures were dried separately in a single diffusion dryer and the flow streams merged immediately before the electrostatic classifier and DMA (TSI 3080 electrostatic classifier with TSI 3081 long column DMA and TSI 3087 aerosol neutralizer).[19] Soot aerosols were generated using a Santoro-style diffusion burner[20] and then transported directly to the DMA.

As discussed above, the DMA size selects particles by their size- and shape-dependent electrical mobility, while the APM (Kanomax model 3601)[19] selects by their mass. For some of the experiments reported here, aerosols were first size selected using a custom-configured electrostatic classifier (TSI 3012 aerosol neutralizer with TSI 3081 long column DMA)[19] and the resulting size distributions measured by the commercially available classifier operated in scanning mode. The CRD and PA spectrometers provided α_{ext} and α_{abs}, respectively. Both instruments were configured from commercially available components; see Supporting Information. Finally, a condensation particle counter (CPC, TSI 3775, high flow mode)[19] was used to measure N.

During single aerosol experiments, the APM was operated in continuous scanning mode. APM voltage and rotation settings were chosen to span the range of masses expected and allow for sufficient aerosol penetration and mass resolution. This balance between penetration and resolution is dictated by the classification parameter which is the ratio of axial to radial transversal times.[21] In keeping with the optimization outlined in Tajima et al.,[22] a classification parameter of 0.32 was used. For the separation of the multiple aerosols, the APM voltage was manually controlled. In both instances, data were logged at 10 Hz using a National Instruments BNC 2120 board, National Instruments GPIB-USB-HS cable and LabView 8.6 virtual instruments written in our lab.[19] Data were averaged to 1 Hz prior to further processing.

Significant literature exists on the use of cavity ring-down spectroscopy (CRDS) for the determination of aerosol extinction coefficients and photoacoustic spectroscopy (PAS) for the determination of aerosol absorption coefficients. For more details, we refer the reader to Atkinson's[23] discussion of CRDS and to articles by Haisch,[24] Havey et al.,[25] or Lack et al.[26] for background on PAS. A brief description is also provided in the Supporting Information.

RESULTS AND DISCUSSION

Calculation of MEC and MAC of Mass-Selected Aerosols. The APM can be operated in either a continuously scanning mode or a stepwise scanning mode; in the continuous mode, the voltage is constantly increasing while the rotation speed is held constant. In stepwise scanning mode, the voltage and rotation speed are set for a desired integration time after which the voltage is changed to measure a different mass. The primary difference between the two modes is that CPC, CRD, and PAS measure dN/dm_{p}, $d\alpha_{\text{ext}}/dm_{\text{p}}$, $d\alpha_{\text{abs}}/dm_{\text{p}}$ in continuous mode, respectively, while N and α_{ext} and a_{abs}, respectively, are measured at fixed mass, m_{p}, in stepwise mode. In either case, we assume that the resulting mass distribution has a Gaussian distribution with respect to N, M, α_{abs}, or α_{ext}. For the remaining derivations, a stepwise scan will be assumed. The number density distribution of masses is

$$N_{\text{m}} = A_{\text{N}} \exp\left(\frac{-(m_{\text{p}} - m_{\text{x}})^2}{2\sigma_{\text{x}}^2}\right) \tag{7}$$

where A_{N} is the peak amplitude, m_{x} is the apparent average mass of the peak, and σ_{x} is the apparent $e^{-1/2}$ halfwidth of the distribution; the actual average mass and halfwidth are qm_{x} and $q\sigma_{\text{x}}$, respectively, where q is the charge. In the case where multiple peaks are present, then the distribution is fit with a summation of Gaussian distributions, and m_{x} and σ_{x} represent the average apparent mass and apparent halfwidth of the peak under investigation. Identical equations can be derived for extinction, absorption and mass concentration by replacing N with α_{ext}, α_{abs}, or M, respectively, where the mass concentration at a given mass is

$$M_{\text{m}} = qm_{\text{p}}N_{\text{m}} \tag{8}$$

From Gaussian fits of the mass concentration and absorption distributions, the mass-specific absorption cross section is

$$\text{MAC} = \frac{\alpha_{\text{abs}}}{M} = \frac{A_{\alpha_{\text{abs}}}\sigma_{\text{abs}}}{A_{\text{M}}\sigma_{\text{M}}} \tag{9}$$

Single Aerosol Separation by Charge. The multiple-charging effects by the DMA on ammonium sulfate aerosol (AS) were investigated and shown in Figure 2. The underlying assumptions and calculations used and numerical results in

dx.doi.org/10.1021/ac401645y | Anal. Chem. 2013, 85, 8319−8325

tabular form (Tables S-1 to S-4) can be found in Supporting Information.

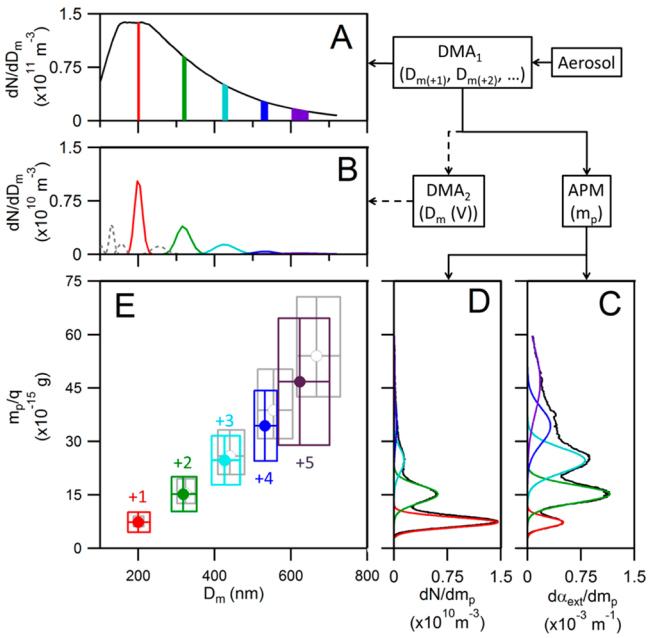

Figure 2. Schematic of aerosol separation by electrical mobility (using a DMA) and mass (using an APM) with optical and concentration measurements. A base size distribution is shown in panel A. This aerosol is then size selected at 200 nm by a DMA. Because of charge coincidence, larger particles with the same electrical mobility are also transmitted (panel B) as measured using a second DMA. Here, +2, +3, +4, and +5 charges correspond to green, cyan, blue, and purple, respectively. In panels C and D, the mass distributions in extinction and concentration as measured by the CRD and CPC, respectively, are shown. Panel E shows the overlap of the separation mechanisms between the DMA and APM; particle masses sorted by the APM emerge at different apparent masses (m_p/q) even though they have the same electrical mobility. Here, the dots represent the peak centers in diameter (D_m) and mass (m_p) and the width of error boxes are the respective $e^{-1/2}$ halfwidths of each peak. The gray circles/boxes represent the theoretical mobility diameters and masses assuming spherical particles with crystalline density.

The base size distribution for the AS aerosol is shown in Figure 2A. This aerosol was size selected to a mobility diameter of 200 nm using a DMA. The distribution of particles with the same electrical mobility through the DMA was measured using an additional DMA and a CPC (Figure 2B). From this figure, it is evident that particles larger than the singly charged 200 nm are also transmitted, corresponding to those with q = +2, +3, +4, and +5. The distributions for the multiply charged particles are shown by the green, cyan, blue, and purple traces. The respective mobility diameters for the q = +1 through +5 particles range from 197.2 to 614.2 nm and are given in Table 1. The gray lines in Figure 2B correspond to particles that are also present in the tandem-DMA distribution due to charge redistribution in the second DMA.

In panels C and D of Figure 2, the measured extinction and number concentration mass distributions are shown, respectively. In terms of concentration, the greatest fractional contribution (f_N) is from the +1 charge (46.3%) as seen in Table 1. However, singly charged (+1) particles represent the lowest fractional contribution in both mass concentration (f_M) and extinction (f_α) at 10.8% and 8.0%, respectively. This small contribution of the singly charged particles toward total mass concentration would result in gross underestimation of the total mass concentration if only the singly charged particles were considered without evaluation of the entire distribution. Further, the optical cross section would be grossly overestimated if the total extinction was assumed to arise from the singly charged particle. With regard to particles with $q \geq 3$, measurement uncertainty is dictated by particle counting statistics. This in turn affects the ability constrain the Gaussian fits of these charges, thereby increasing uncertainty in particle concentrations. This error then propagates to mass concentration and mass extinction measurements as illustrated in Table 1 for q = +4 and +5.

The overlap of DMA and APM separation mechanisms for AS was calculated theoretically and from the measured size and mass distributions and is shown in Figure 2E. The dots represent the center of the measured distributions in diameter and apparent mass (m_p/q) while the error boxes represent the $e^{-1/2}$ halfwidth of the distribution. The gray boxes represent the theoretical separation of these particles assuming sphericity, crystalline density (1.77 g/cm^3), and a 1:1 mapping of the transfer functions of the DMA and APM. This latter assumption is not expected to be completely valid because the APM likely causes some broadening of the aerosol distribution that exits the DMA.[21] From Figure 2E, it is evident that the combined DMA-APM system effectively separates all particles exiting the DMA because the charge coincidence problems of the two component instruments do not overlap; see eq 5.

The separation by mass of a single-component electrostatically classified aerosol stream can be extended beyond the AS shown here. For highly irregular aerosols with large Cunningham slip correction factors, like soot, a high degree of overlap exists between the +1 particle of interest and higher-order charges, even after electric mobility and mass separation. Under these conditions, the presence of an optical measurement allows for discrimination as a function of charge because optical

Table 1. Fractional Number Concentration, Fractional Mass Concentration, Fractional Extinction (α), and Mass Extinction Coefficients and Their Respective Uncertainties (u) for Ammonium Sulfate as a Function of Charge for Particles with an Equivalent 200 nm Electrical Mobility Diameter[a]

q	$f_N = N/N_{tot}$ (%)	$u(f_N)$ (%)	$f_M = M/M_{tot}$ (%)	$u(f_M)$ (%)	$f_\alpha=\alpha/\alpha_{tot}$ (%)	$u(f_\alpha)$ (%)	MEC (m^2/g)	u(MEC) (m^2/g)
1	46.3	3.4	10.8	2.3	7.96	0.74	4.24	0.09
2	35.5	2.9	28.5	6.2	31.65	2.9	6.36	0.41
3	11.1	2.4	17.9	7.3	31.42	3.38	10.04	6.92
4	4.4	3.6	29.4	18.9	18.12	7.51	3.53	4.49
5	2.7	5.4	13.4	11.1	10.84	5.07	4.65	7.73

[a]Uncertainties are calculated from propagation of errors in Gaussian fits (k = 2).

dx.doi.org/10.1021/ac401645y | Anal. Chem. 2013, 85, 8319−8325

cross sections depend upon particle size. Without this optical cross section measurement, this discrimination would not be possible.

Multiple Aerosol Separation. The DMA-APM-CRD/PA-CPC enables the separation of multiple aerosols within a single source stream by exploiting differences in density and/or optical properties. Under other experimental configurations where the APM is not used—i.e. DMA only, CRD only, or tandem DMA-CRD—multiple species cannot be separated.

To illustrate our ability to separate multiple species, we selected two materials with large differences in effective densities and optical properties, NaCl and graphene oxide (GO). We previously showed that GO forms aerosols with a structure similar to crumpled paper and through thermal reduction it can be optically tuned to mimic brown to black-like carbon.[27] Here GO was reduced at 350 °C to obtain a strongly absorbing aerosol that could be paired with the strongly scattering and nonabsorbing NaCl. The GO aerosol stream was merged with the polydisperse NaCl aerosol prior to size selection by the DMA. The combined aerosol stream was size selected at D_m = 250 nm.

Figure 3 shows the results of the number concentration (top) and corresponding extinction and absorption coefficient

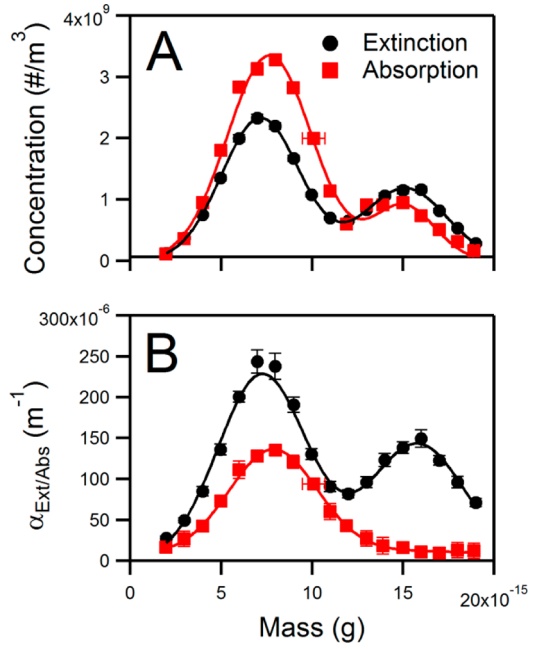

Figure 3. Number concentration (top) and optical coefficients (bottom) measured during extinction (black dots) and absorption (red squares) mass scans of a 250 nm size selected external mixture of NaCl and GO reduced at 350 °C.

(bottom) scans as a function of mass. The peaks on the left and right correspond to reduced GO and NaCl, which have effective densities of 1 g/cm^3 and 1.8 g/cm^3, respectively. In this figure, the two aerosols are separated in the mass distribution as evidenced by the peaks at 7.7 × 10^{-15} g and 15 × 10^{-15} g. No conclusions about the identity or other properties of these aerosols can be drawn from the mass distribution alone. However, from the absorption and extinction plots (bottom) and the calculated MAC and MEC in Table 2, it is evident that two distinct aerosols are present; the graphene oxide displays significantly stronger absorption

Table 2. MAC and MEC of Graphene Oxide and NaCl Aerosols Determined from Figure 3[a]

	MAC (m^2/g)	u(MAC) (m^2/g)	MEC (m^2/g)	u(MEC) (m^2/g)	ω_0	u(ω_0)
GO	7.5	1.65	15.71	1.15	0.52	0.11
NaCl	0	0	8.93	1.22	1	
other	1.19[b]	0.56[b]				

[a]Uncertainties are calculated from propagation of errors in Gaussian fits (k = 2). [b]The residual absorption present in the NaCl data is attributed to residual nigrosin present within the atomizer.

than the NaCl. The NaCl absorption trace does display some residual absorption, but this is attributed to a small amount of residual nigrosin contamination in the atomizer.

Aerosol Speciation by Density. To test the effectiveness of classifying aerosols, the mass specific absorption and extinction coefficients of different classes of aerosols (organic, inorganic, strongly absorbing, weakly absorbing and strongly scattering) were collected at a mobility diameter of 250 nm. The aerosols investigated consisted of soot generated from an ethylene flame, particles generated from aqueous solutions of nigrosin dye, AS, aquarium salt (sea salt surrogate), $NaNO_3$, Na_2SO_4, and GO reduced to various degrees in a temperature programmable tube furnace.[27] The MAC and MEC were determined by collecting a concentration-dependent mass distribution and then collecting CRD and PA data at the peak of the distribution. The resulting MAC and MEC are presented at the bottom of Figure 4 while the single-scattering albedo, ω_0, is shown in the top. The strongly scattering aerosols are shown in red, GO in green, nigrosin in blue, and soot in black. The MAC for the salts has been omitted as it is essentially 0; all have albedos of approximately 1. The solid gray lines segregate low (0−1 g/cm^3), intermediate (1−2 g/cm^3), and high (>2 g/cm^3) density as previously assigned.[28]

The MAC and MEC of the investigated aerosols are presented as a function of effective density in Figure 4. All of the salts have intermediate-to-high effective densities, low mass extinctions (~10 m^2/g or less), and no mass absorption. The GO aerosol exhibits increasing MEC and MAC and decreasing albedo with decreasing effective density. This density decrease corresponds to the loss of material associated with GO thermal reduction and is consistent with other observations of GO.[27] BC exhibits relatively high MAC and MEC values. These results are attributable to the low effective density and fractal morphology of soot which makes it an effective mass absorber. For the 250 nm mobility diameter used here, there is a weak inverse correlation between absorption and extinction cross sections and particle density. However, we interpret this result as being coincidental because all the particles happen to possess similar cross sections at this mobility diameter. This can be understood in terms of eq 2 where C_{abs} and V are treated as constants. However, this trend would not be expected if a larger set of particle types and sizes were considered.

Park et al. 2008, presented the effective density of urban aerosols from multiple field campaigns. They speculated that the low density particles were probably composed of primary agglomerates of soot, while the intermediate density particles likely corresponded to organic/sulfate mixed particles. From the data presented in Figure 4, it is evident that the low-density particles could be composed of soot agglomerates.[29] However, it is also possible that organic particles could be present in this range, if one considers GO to be representative of so-called

dx.doi.org/10.1021/ac401645y | Anal. Chem. 2013, 85, 8319−8325

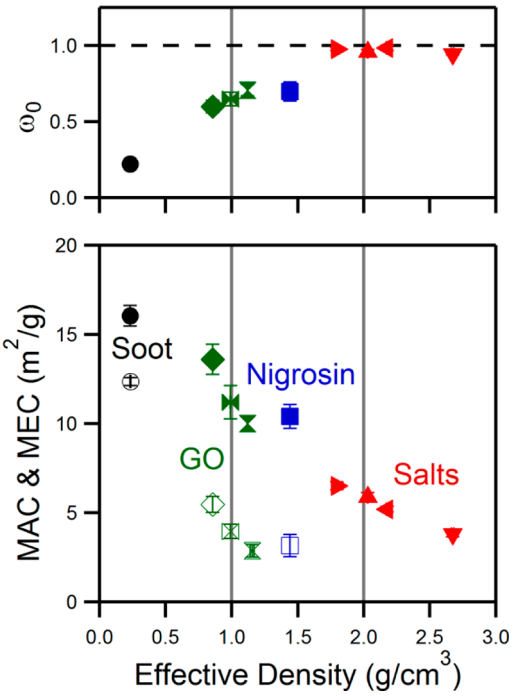

Figure 4. Plots of single-scattering albedo (top) and mass extinction and mass absorption coefficients (bottom) versus effective density for different aerosol species with a mobility diameter of 250 nm: AS (red triangle pointing right) aquarium salt (red triangle pointing up), $NaNO_3$ (red triangle pointing down), Na_2SO_4 (red triangle pointing left), reduced GO at 200 °C (green vertical bowtie), 250 °C (green horizontal bowtie), and 300 °C (green diamond), nigrosin (blue square), and soot (black circle). The solid markers represent extinction while the open markers represent absorption. Uncertainties are calculated from propagation of standard deviations in mass and extinction/absorption (k = 2).

"brown carbon"[7a] present in the atmosphere; we draw this correlation loosely on the basis that GO can exhibit a range of optical properties and densities similar to brown carbon particles.[27] The technique presented herein has the potential to separate BC from other materials. In the Intermediate density range, we found the strongly scattering salts and nigrosin, which implies that particles in this range can exhibit a wide range of optical properties. In the ambient atmosphere, hygroscopic aerosols,[30] aged carbonaceous aerosols,[31] secondary organic aerosols,[32] and polluted maritime aerosol[33] have been shown to occupy this range. Further, from our data, the aquarium salt, $NaNO_3$, and Na_2SO_4 particles fall within the high density category. This density range has been attributed to high density salts, sea spray or crustal materials,[34] or fly ash from coal fired power plants.[35] Some caution in the interpretation of these data should be taken because these results are for laboratory-generated aerosols, while all other sources were for ambient aerosols.

CONCLUSIONS

We have demonstrated the direct measurement of mass extinction and mass absorption coefficients of laboratory-generated aerosols using a combination of mobility and mass analyzers in conjunction with absorption and extinction laser spectrometers and particle counting methods. This suite of instruments can be used to measure mass-specific optical cross sections for particles with densities similar to those in the urban atmosphere. Compared to the performance of any of the component methods used on its own or in any paired combination, the complete set of size, mass, extinction, absorption, and concentration measurements described here improves particle selectivity and reduces the uncertainty of aerosol optical properties.

ASSOCIATED CONTENT

Supporting Information

This section contains additional text and equations describing the use of cavity ring-down spectroscopy and photoacoustic spectroscopy and the calculation of particle diameters and masses as a function of charge for the DMA-APM system. This material is available free of charge via the Internet at http://pubs.acs.org.

AUTHOR INFORMATION

Corresponding Author

*Phone: (301) 975-8709. E-mail: Christopher.Zangmeister@nist.gov.

Notes

The authors declare no competing financial interest.

REFERENCES

(1) Kleinstreuer, C.; Zhang, Z.; Donohue, J. F. *Annu. Rev. Biomed. Eng.* **2008**, *10*, 195−220.

(2) Darquenne, C. *J. Aerosol Med. Pulm. Drug Delivery* **2012**, *25*, 140−147.

(3) Mahowald, N.; Ward, D. S.; Kloster, S.; Flanner, M. G.; Heald, C. L.; Heavens, N. G.; Hess, P. G.; Lamarque, J.-F.; Chuang, P. Y. *Annu. Rev. Environ. Resour.* **2011**, *36*, 45−74.

(4) (a) Jacobson, M. Z. *Nature* **2001**, *409*, 695−697. (b) Bond, T. C.; Doherty, S. J.; Fahey, D. W.; Forster, P. M.; Berntsen, T.; DeAngelo, B. J.; Flanner, M. G.; Ghan, S.; Kärcher, B.; Koch, D.; Kinne, S.; Kondo, Y.; Quinn, P. K.; Sarofim, M. C.; Schultz, M. G.; Schulz, M.; Venkataraman, C.; Zhang, H.; Zhang, S.; Bellouin, N.; Guttikunda, S. K.; Hopke, P. K.; Jacobson, M. Z.; Kaiser, J. W.; Klimont, Z.; Lohmann, U.; Schwarz, J. P.; Shindell, D.; Storelvmo, T.; Warren, S. G.; Zender, C. S. *J. Geophys. Res.: Atmos.* 2013, doi: 10.1002/jgrd.50171. (c) Moffet, R. C.; Prather, K. A. *Proc. Natl. Acad. Sci. U.S.A.* **2009**, *106*, 11872−11877. (d) Ramanathan, V.; Carmichael, G. *Nature Geosci* **2008**, *1*, 221−227.

(5) Sato, M.; Hansen, J.; Koch, D.; Lacis, A.; Ruedy, R.; Dubovik, O.; Holben, B.; Chin, M.; Novakov, T. *Proc. Natl. Acad. Sci. U.S.A.* **2003**, *100*, 6319−6324.

(6) (a) Hansen, A. D. A.; Rosen, H.; Novakov, T. *Sci. Total Environ.* **1984**, *36*, 191−196. (b) Bond, T. C.; Anderson, T. L.; Campbell, D. *Aerosol Sci. Technol.* **1999**, *30*, 582−600.

(7) (a) Andreae, M. O.; Gelencser, A. *Atmos. Chem. Phys.* **2006**, *6*, 3131−3148. (b) Arnott, W. P.; Moosmüller, H.; Sheridan, P. J.; Ogren, J. A.; Raspet, R.; Slaton, W. V.; Hand, J. L.; Kreidenweis, S. M.; Collett, J. L. *J. Geophys. Res.: Atmos.* **2003**, *108*, AAC 15−1−AAC 15−11.

(8) (a) Kirchstetter, T. W.; Corrigan, C. E.; Novakov, T. *Atmos. Environ.* **2001**, *35*, 1663−1671. (b) Subramanian, R.; Roden, C. A.; Boparai, P.; Bond, T. C. *Aerosol Sci. Technol.* **2007**, *41*, 630−637. (c) Moosmüller, H.; Chakrabarty, R. K.; Arnott, W. P. *J. Quant. Spectrosc. Radiat. Transfer* **2009**, *110*, 844−878. (d) McInnes, L. M.; Quinn, P. K.; Covert, D. S.; Anderson, T. L. *Atmos. Environ.* **1996**, *30*, 869−884.

(9) Schnaiter, M.; Horvath, H.; Möhler, O.; Naumann, K. H.; Saathoff, H.; Schöck, O. W. *J. Aerosol Sci* **2003**, *34*, 1421−1444.

(10) (a) Levin, E. J. T.; McMeeking, G. R.; Carrico, C. M.; Mack, L. E.; Kreidenweis, S. M.; Wold, C. E.; Moosmüller, H.; Arnott, W. P.; Hao, W. M.; Collett, J. L., Jr.; Malm, W. C. *J. Geophys. Res.* **2010**, *115*, D18210. (b) Bond, T. C.; Bergstrom, R. W. *Aerosol Sci. Technol.* **2006**, *40*, 27−67.

(11) Subramanian, R.; Kok, G. L.; Baumgardner, D.; Clarke, A.; Shinozuka, Y.; Campos, T. L.; Heizer, C. G.; Stephens, B. B.; de Foy, B.; Voss, P. B.; Zaveri, R. A. *Atmos. Chem. Phys.* **2010**, *10*, 219−237.
(12) Slowik, J. G.; Cross, E. S.; Han, J.-H.; Davidovits, P.; Onasch, T. B.; Jayne, J. T.; Williams, L. R.; Canagaratna, M. R.; Worsnop, D. R.; Chakrabarty, R. K.; Moosmüller, H.; Arnott, W. P.; Schwarz, J. P.; Gao, R.-S.; Fahey, D. W.; Kok, G. L.; Petzold, A. *Aerosol Sci. Technol.* **2007**, *41*, 295−314.
(13) Knutson, E. O.; Whitby, K. T. *J. Aerosol Sci.* **1975**, *6*, 443−451.
(14) (a) Kulkarni, P.; Baron, P. A.; Willeke, K. *Aerosol Measurement: Principles, Techniques, and Applications*, 3rd ed.; John Wiley & Sons, Inc.: Hoboken, NJ, 2011. (b) Kelly, W. P.; McMurry, P. H. *Aerosol Sci. Technol.* **1992**, *17*, 199−212.
(15) Wang, Z.; King, S. M.; Freney, E.; Rosenoern, T.; Smith, M. L.; Chen, Q.; Kuwata, M.; Lewis, E. R.; Pöschl, U.; Wang, W.; Buseck, P. R.; Martin, S. T. *Aerosol Sci. Technol.* **2010**, *44*, 939−953.
(16) Park, K.; Kittelson, D.; McMurry, P. *Aerosol Sci. Technol.* **2004**, *38*, 881−889.
(17) Ehara, K.; Hagwood, C.; Coakley, K. J. *J. Aerosol Sci.* **1996**, *27*, 217−234.
(18) (a) McMurry, P. H.; Wang, X.; Park, K.; Ehara, K. *Aerosol Sci. Technol.* **2002**, *36*, 227−238. (b) Barone, T. L.; Lall, A. A.; Storey, J. M. E.; Mulholland, G. W.; Prikhodko, V. Y.; Frankland, J. H.; Parks, J. E.; Zachariah, M. R. *Energy Fuels* **2011**, *25*, 1978−1988. (c) Liu, Q.; Ma, X.; Zachariah, M. R. *Microporous Mesoporous Mater.* **2012**, *153*, 210−216. (d) Park, K.; Kittelson, D.; Zachariah, M.; McMurry, P. *J. Nanopart. Res.* **2004**, *6*, 267−272. (e) Qiu, C.; Khalizov, A. F.; Zhang, R. *Environ. Sci. Technol.* **2012**, *46*, 9464−9472.
(19) NIST Technical Disclaimer: Certain commercial equipment, instruments, or materials (or suppliers, or software, ...) are identified in this paper to foster understanding. Such identification does not imply recommendation or endorsement by the National Institute of Standards and Technology, nor does it imply that the materials or equipment identified are necessarily the best available for the purpose.
(20) Santoro, R. J.; Semerjian, H. G.; Dobbins, R. A. *Combust. Flame* **1983**, *51*, 203−218.
(21) Lall, A. A.; Ma, X.; Guha, S.; Mulholland, G. W.; Zachariah, M. R. *Aerosol Sci. Technol.* **2009**, *43*, 1075−1083.
(22) Tajima, N.; Fukushima, N.; Ehara, K.; Sakurai, H. *Aerosol Sci. Technol.* **2011**, *45*, 196−214.
(23) Atkinson, D. B. *Analyst* **2003**, *128*, 117−125.
(24) Haisch, C. *Meas. Sci. Technol.* **2012**, *23*, 012001.
(25) Havey, D. K.; Bueno, P. A.; Gillis, K. A.; Hodges, J. T.; Mulholland, G. W.; van Zee, R. D.; Zachariah, M. R. *Anal. Chem.* **2010**, *82*, 7935−7942.
(26) Lack, D. A.; Lovejoy, E. R.; Baynard, T.; Pettersson, A.; Ravishankara, A. R. *Aerosol Sci. Technol.* **2006**, *40*, 697−708.
(27) Ma, X.; Zachariah, M. R.; Zangmeister, C. D. *J. Phys. Chem. C* **2013**, *117*, 3185−3191.
(28) Park, K.; Dutcher, D.; Emery, M.; Pagels, J.; Sakurai, H.; Scheckman, J.; Qian, S.; Stolzenburg, M. R.; Wang, X.; Yang, J.; McMurry, P. H. *Aerosol Sci. Technol.* **2008**, *42*, 801−816.
(29) Spencer, M. T.; Shields, L. G.; Prather, K. A. *Environ. Sci. Technol.* **2007**, *41*, 1303−1309.
(30) Stein, S. W.; Turpin, B. J.; Cai, X.; Huang, P.-F.; McMurry, P. H. *Atmos. Environ.* **1994**, *28*, 1739−1746.
(31) Pitz, M.; Cyrys, J.; Karg, E.; Wiedensohler, A.; Wichmann, H. E.; Heinrich, J. *Environ. Sci. Technol.* **2003**, *37*, 4336−4342.
(32) Malloy, Q. G. J.; Nakao, S.; Qi, L.; Austin, R.; Stothers, C.; Hagino, H.; Cocker, D. R. *Aerosol Sci. Technol.* **2009**, *43*, 673−678.
(33) Geller, M.; Biswas, S.; Sioutas, C. *Aerosol Sci. Technol.* **2006**, *40*, 709−723.
(34) Hänel, G.; Thudium, J. *PAGEOPH* **1977**, *115*, 799−803.
(35) Ghosal, S.; Self, S. A. *Fuel* **1995**, *74*, 522−529.